SUPERNOVA HYDRODYNAMICS EXPERIMENTS ON THE NOVA LASER

B. A. Remington — *R. London* — *D. Arnett*[***] — *J. Kane*[***]

J. Castor — *E. Liang*[**] — *R. P. Drake*[†] — *R. J. Wallace*

R. McCray[*] — *S. G. Glendinning* — *L. J. Suter* — *A. Rubenchik*[†††]

K. Estabrook — *D. H. Munro* — *B. Fryxell*[††]

Introduction

In studying complex astrophysical phenomena, such as supernovae (SNs), investigators do not have the luxury of setting up well controlled experiments at some distant location in the universe to test the physics of their models and theories. A surrogate environment to serve as an experimental astrophysics testbed would be highly beneficial. Sophisticated, modern research lasers have been developed largely as a result of the world-wide effort in inertial confinement fusion. Such lasers offer the potential for creating just such an experimental testbed using well controlled, well diagnosed laser-produced plasmas.

On February 23, 1987, at 0735 UT, the blue supergiant Sanduleak located in the Large Magellanic Cloud, a dwarf galaxy at a distance of 50 kpc from earth, exploded as a core-collapse Type II supernova (SN).[1] This event was marked by a prodigious outburst of neutrinos followed ~3 h later by the ultraviolet (UV) flash as the shock broke through the surface of the star. Thus began what will certainly be recorded as the most significant astrophysical event of the decade.

By February 23, 1997, SN1987A will have been studied for 10 years, and our understanding has progressed enormously. One example is the consensus that strong hydrodynamic mixing of the heavier core elements outward into the lower-density envelope is needed to explain a wide range of observables. Figure 1(a), which shows the results from a two-dimensional (2-D) simulation of SN1987A at 3.6 h after explosion, is an image of density to illustrate such mixing.[2] However, new mysteries continue to emerge. Despite considerable effort worldwide, simulations still predict that the mixing front progresses significantly more slowly than is actually observed.[3–8]

SN1987A is now evolving into the early remnant stage. Figure 1(b) shows an optical image taken in February 1994 with a wide-field camera on the Hubble Space Telescope (HST).[9] The expanding SN ejecta corresponds to the central bright spot, surrounded by what appears to be an assembly of three rings. The origin of these ring nebulae remains a mystery.[10] There is general agreement, however, that the SN ejecta is expanding at a much greater velocity (~10^4 km/s) than the nebular rings (10–20 km/s), with the ejecta expected to impact the inner ring in 5 to 10 years.[10–16] We stand poised to witness a colliding plasma "astrophysics experiment" of a spectacular nature. Simulations offer enticing glimpses of what may happen, as shown by the density–pressure plots in Figures 1(c) and 1(d) (reproduced from Ref. 16). Apart from cosmic pyrotechnics, this collision may shed light on the nature of the circumstellar ring nebula.

Both of these phases of SN evolution—the core hydrodynamic mixing at intermediate times (10^3–10^4 s), and colliding plasmas during remnant formation—are areas rich with possibilities for supporting laboratory experiments. This article describes two such experiments using the Nova laser[17] at LLNL to create the relevant plasma environment. First, we discuss hydrodynamic instabilities in the context of core-collapse SNs (in particular, SN1987A) and the corresponding laser experiment. Next, we describe the early stages of SN1987A remnant formation and the corresponding laser experiment. We conclude with an outlook for the future.

* University of Colorado, Boulder, Colorado.
** Rice University, Houston, Texas.
*** University of Arizona, Tucson, Arizona.
† University of Michigan, Ann Arbor, Michigan.
†† George Mason University, Fairfax, Virginia.
†††University of California, Davis, California.

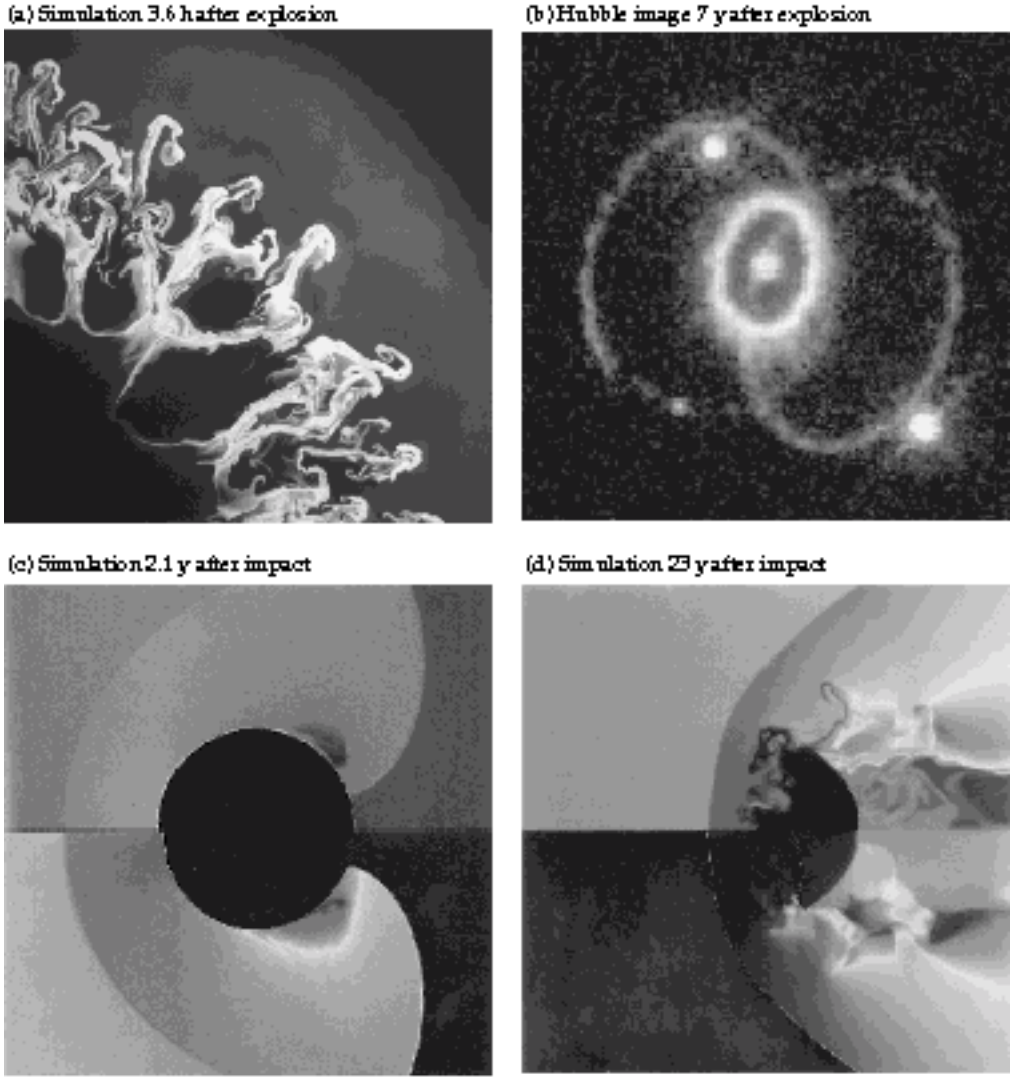

FIGURE 1. (a) Result, in terms of density, from a 2-D simulation of the hydrodynamic mixing in SN1987A (reproduced from Ref. 2). The initial velocity perturbation was $\delta v/v = 10\%$. (b) Image of SN1987A obtained by the Hubble Telescope in February 1994 (reproduced from Ref. 9). The expanding SN ejecta is the central dot. The inner, yellow ring is a planetary nebula of uncertain origin. The outer rings are also part of the nebular structure. The emissions have now faded but are expected to resume in a few years when the ejecta strike the inner ring. (c) Simulations of the collision of SN ejecta with the inner ring nebula two years after initial impact (from Ref. 16). The top half represents density; the bottom half is pressure. (d) Same as (c), except 23 years after initial impact. (40-00-1296-2753pb01)

Hydrodynamics of SN1987A

The first hints that all was not well with a spherically symmetric, one-dimensional (1-D) model of SN1987A came from the light curve (total luminosity vs time). A secondary maximum was observed, but it was considerably earlier (~20 days) and broader than expected.[18] Then came the "Bochum event," a spectroscopic anomaly starting at day ~25 and suggesting an auxiliary heat source.[19] The observation of the core elements ^{56}Ni, ^{56}Co, and ^{56}Fe poking out through the surrounding hydrogen envelop six months earlier than expected, however, proved conclusive.[10,20] The 1-D models of SNs were largely abandoned, and modeling in 2D commenced in earnest. From the Doppler broadening of the infrared and gamma spectral lines of Fe, Ni, and Co, core velocities as great as 3000 km/s were inferred.[20] Modeling (done primarily in 2D) predicts significantly lower peak velocities.[2,3] It would be highly beneficial to be able to experimentally test the hydrodynamic instability modeling of the SN codes.

Current uncertainties notwithstanding, the following picture has emerged for SN1987A. A 1-D stellar evolution calculation gives the density profile for the 19-$M_\odot$ mass progenitor,[21] shown in Figure 2(a), where $M_\odot$ represents one solar mass. An inner Fe core, $M_r/M_\odot < 1.6$, is surrounded by a layer of Si, Ne, O, and C in the region corresponding to $1.6 < M_r/M_\odot < 2.3$, where M_r is the mass out to a radius r. This layer is followed by a mostly He layer at $2.3 < M_r/M_\odot < 6$, ending in a hydrogen envelope for $M_r/M_\odot > 6$, which extends out to a radius of $R_0 = 2.2 \times 10^{12}$ cm. The SN explosion is triggered when the Fe core collapses to form a 1.6-$M_\odot$ neutron star. When the core reaches the density of nuclear degenerate matter, the core rebounds, which launches an exceedingly strong radial shock propagating outward through the star, corresponding to a release of $1–2 \times 10^{51}$ ergs of energy, which effectively blows the star apart. The mass cut—that is, the division between what collapses into the neutron star versus what is ejected—is believed to lie somewhere within the oxygen layer.

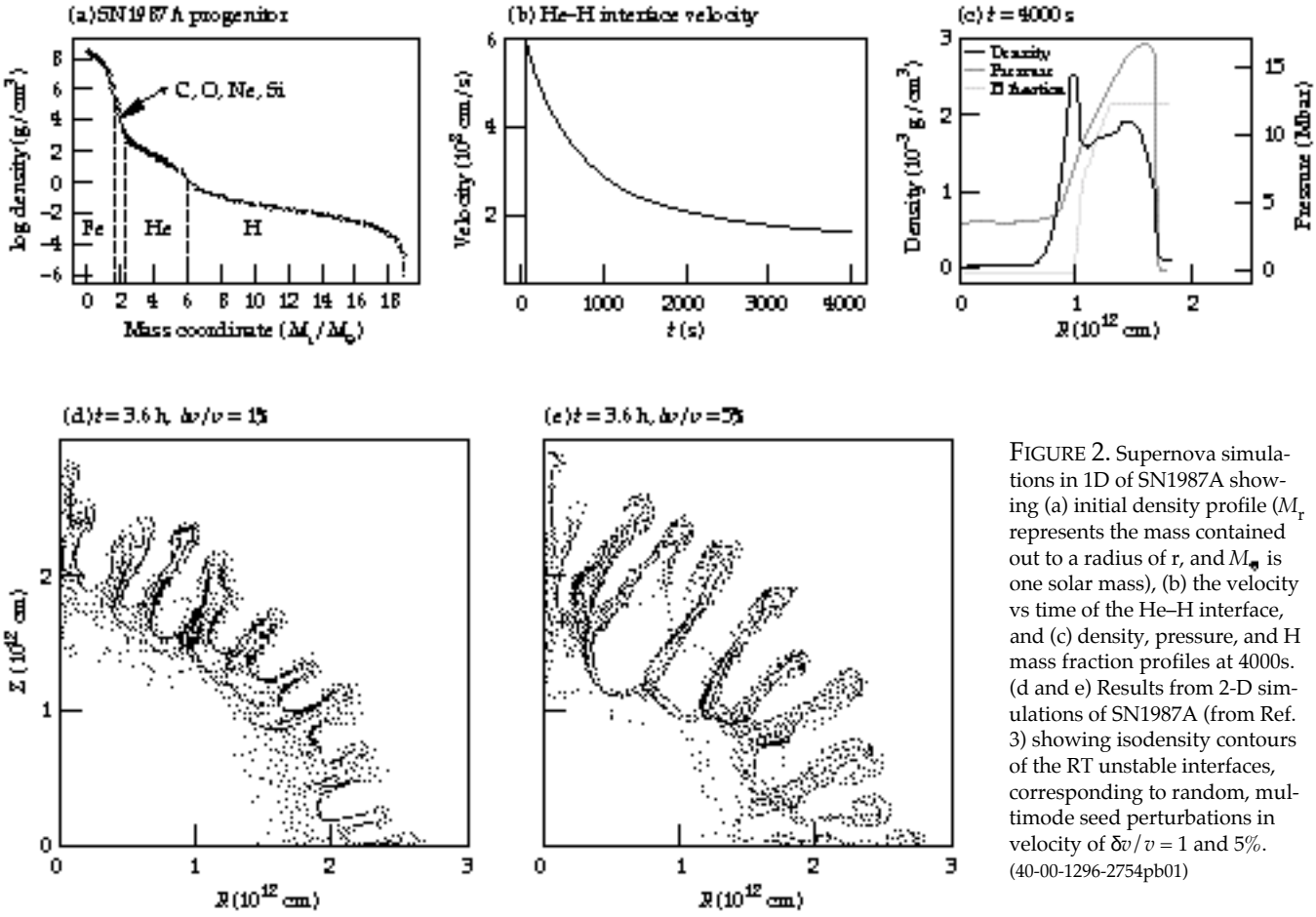

FIGURE 2. Supernova simulations in 1D of SN1987A showing (a) initial density profile (M_r represents the mass contained out to a radius of r, and $M_\odot$ is one solar mass), (b) the velocity vs time of the He–H interface, and (c) density, pressure, and H mass fraction profiles at 4000s. (d and e) Results from 2-D simulations of SN1987A (from Ref. 3) showing isodensity contours of the RT unstable interfaces, corresponding to random, multimode seed perturbations in velocity of $\delta v/v = 1$ and 5%. (40-00-1296-2754pb01)

We start with a progenitor similar to that shown in Figure 2(a) and calculate the hydrodynamic evolution using the SN hydrodynamics code PROMETHEUS.[3,22] In this work, we focus on instabilities at the He–H interface. To economize computing time, we model only $M_r/M_\odot \geq 5$, depositing the explosion energy, $E = 1.5 \times 10^{51}$ ergs, as a mix of thermal and kinetic energy at the inner boundary ($M_r/M_\odot = 5$). This launches a strong radial shock that reaches the He–H interface ($M_r/M_\odot = 6$) after a transit time of about 100 s. At this point, the initial density, pressure, temperature, and velocity at the interface are 2.3 g/cm^3, 75 Gbar, 6 keV, and 6×10^8 cm/s, respectively. Figure 2(b) shows the velocity of the He–H interface as a function of time, and Figure 2(c) shows the density and pressure profiles at a time of 4000 s. By 4000 s, the shock has traveled about halfway out of the star. Note that at the He–H interface ($R \approx 1.0 \times 10^{12}$ cm), the pressure and density gradients are crossed, that is, $\nabla\rho \cdot \nabla P < 0$, such that the He layer is being decelerated by the H layer. This situation is unstable to the Rayleigh–Taylor (RT) instability,[23] and perturbations at the interface grow in time.

The evolution of compressible, nonlinear, multimode RT instability is an unsolved theoretical problem, and detailed numerical simulations are required. An example of a typical 2-D SN simulation is shown in Figures 2(d) and 2(e) by the isodensity contours corresponding to a time of 3.6 h (Ref. 3). The two cases shown here differ only in the magnitude of the initial multimode velocity perturbation: $\delta v/v = 1\%$ and 5%. [Note that the calculation shown in Figure 1(a) is similar, except that the resolution is higher by a factor of 2, and $\delta v/v = 10\%$]. Strong instability growth is evident, with spikes of the heavier He falling radially outward through the lower-density H layer. The following observations are noteworthy. First, the instability has evolved well into the nonlinear regime for all the calculations, with characteristic peak-to-valley amplitudes larger than characteristic wavelengths, $\eta_{PV} \geq \lambda_{char}$, and the perturbations taking on the classic RT bubble-and-spike shape. Second, the final result at 3.6 h is still sensitive to the "initial conditions" because increasing the seed amplitudes increases the growth. Third, there appears to be a characteristic dominant mode of mode number $l = 2\pi R/\lambda \approx 20$, although the starting configuration was a random multimode pattern. Fourth, the peak velocities of the Ni spikes penetrating into the hydrogen envelope in these calculations are not appreciably different, with $v_{max} \leq 2000$ km/s.

Experiments of Supernova Hydrodynamics

Figure 3(a) shows the experimental configuration, described extensively elsewhere,[24–26] for our laser experiments. Eight of the ten Nova laser beams at a duration of 1 ns and total energy of 12 kJ are focused into a 3.0-mm-long, 1.6-mm-diam Au hohlraum (cylindrical radiation cavity) converting to a ~190-eV thermal x-ray drive. The experimental package is planar, with an 85-μm Cu ($\rho = 8.9$ g/cm^3) foil backed by 500 μm of CH_2 ($\rho = 0.95$ g/cm^3). A sinusoidal ripple with wavelength $\lambda = 200$ μm and amplitude $\eta_0 = 20$ μm is imposed at this embedded interface. The package is mounted across a diagnostic hole in the hohlraum wall so that the inner (smooth) side of the Cu sees the x-ray drive. Diagnosis of the interface is through side-on, x-ray radiography using the remaining two Nova beams focused onto an Fe backlighter disk to generate a 5-ns pulse of He-α x rays at 6.7 keV. In this side-on view, the opaque Cu appears as a shadow, and the CH_2 is essentially transparent.

We model the laser experiment using a combination of codes. Figures 3(b) through 3(d) show the results of modeling in 1D with HYADES,[27] CALE,[28] and PROMETHEUS.[3,22] HYADES is a 1-D Lagrangian code with multigroup radiation transport and tabular equation of state (EOS); CALE is a 2-D ALE code with tabular EOS; and PROMETHEUS is a 2-D Eulerian PPM code using (here) an ideal-gas EOS. We use a measured radiation temperature, $T_r(t)$, as the source input to HYADES. Figure 3(b) shows the velocity of the Cu–CH_2 interface as simulated in HYADES. Note the impulsive shock acceleration, followed by a protracted deceleration, similar to that of the He–H interface in the SN shown in Figure 2(b). We do a high-resolution HYADES run, including multigroup radiation transport, for the first 2.45 ns, at which time the shock approaches the Cu–CH_2 interface. We then map the results to either 1-D or 2-D CALE and PROMETHEUS. (We do not have radiation transport in the versions of these 2-D codes that we are using.) We compare the results for pressure and density at 20 ns from a continuous 1-D HYADES run including radiation transport versus that from CALE [Figure 3(c)] and PROMETHEUS [Figure (3d)]. The mapping works very well for both codes. Note that the pressures for the Nova experiment, 1–2 Mbar, are not too different from those of the SN (10–15 Mbar), as shown in Figure 2(c), although the SN densities are lower by a factor of about 10^3.

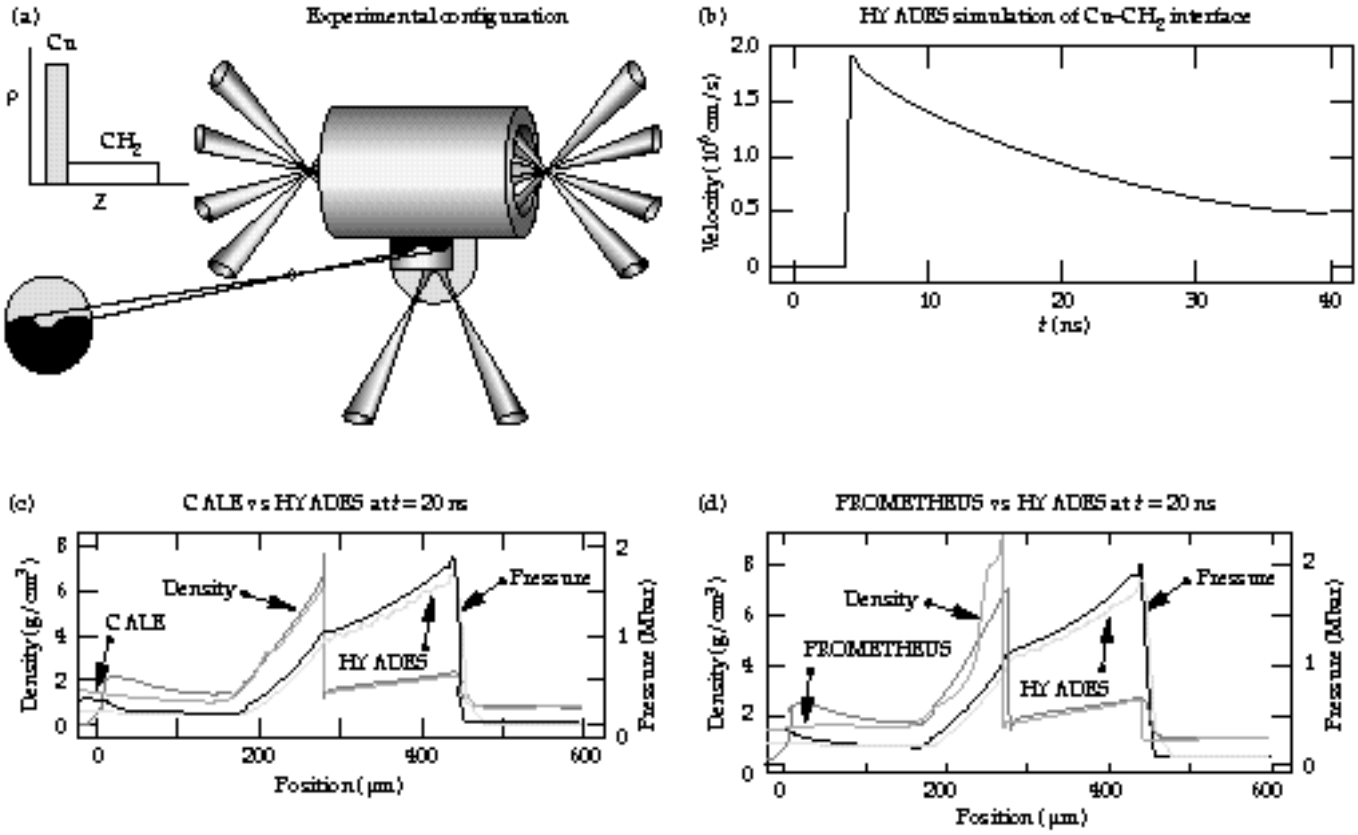

FIGURE 3. SN hydrodynamics experiment using the Nova laser. (a) Experimental configuration. (b) Velocity versus time of the Cu–CH_2 interface from a 1-D HYADES simulation. (c) 1-D simulation showing density and pressure profiles at 20 ns using the codes HYADES and CALE. (d) Same as (c) except using PROMETHEUS instead of CALE. (40-00-1296-2755pb01)

The difference of scales between the SN and the Nova experiment needs to be addressed. We assume the mixing is dominated by the RT instability. In the nonlinear regime, fluid flow can be characterized by a spatial scale on the order of the perturbation wavelength λ, and velocity on the order of the perturbation terminal bubble velocity $v_B \sim (g\lambda)^{1/2}$. Here, g corresponds to the acceleration, and we assume a constant Atwood number. A hydrodynamic time scale is then given by $\tau = \lambda / v_B \sim (\lambda / g)^{1/2}$, and the hydrodynamics equations are invariant under the scale transformation[29] $\lambda \rightarrow a_1\lambda$, $g \rightarrow a_2 g$, and $\tau \rightarrow (a_1/a_2)^{1/2}\tau$. We illustrate this transformation, using characteristic scales taken from the simulations shown in Figures 2 and 3. At 4000 s for the SN, the deceleration of the He–H interface is $g_{SN} = -1.5 \times 10^4$ cm/s^2, the density gradient scalelength is $L_{SN} = \rho/\ \rho = 8 \times 10^{10}$ cm, and the dominant perturbation wavelength is approximated to be $\lambda_{SN} \approx 10 L_{SN} = 8 \times 10^{11}$ cm. For the Nova experiment at 20 ns, $g_{Nova} = -2.5 \times 10^{13}$ cm/s^2, $\lambda_{Nova} = 2 \times 10^{-2}$ cm, and the characteristic time interval is $\tau_{Nova} = 5$ ns. The scale transformation is given by $a_1 = \lambda_{SN}/\lambda_{Nova} = 4 \times 10^{13}$, and $a_2 = g_{SN}/g_{Nova} = 6 \times 10^{-10}$. The corresponding hydrodynamically equivalent time interval for the SN is then given by $\tau_{SN} = (a_1/a_2)^{1/2}\tau_{Nova} = 1.3 \times 10^3$ s, which is an appropriate time scale for the SN instability evolution that we are investigating. (Similar scale transformations across vastly different scales have been demonstrated experimentally before.[30]) Hence, the Nova experiment investigates nonlinear compressible hydrodynamics similar to that at the He–H interface of a Type II SN at intermediate times (10^3–10^4 s).

Figure 4(a) shows a 2-D image from the experiment at 33 ns. These results can be compared with those from the 2-D simulations at 30 ns [Figures 4(b) and 4(c)], both before and after smearing to resemble the effect of the instrumental spatial resolution. The experimentally observed perturbation has evolved into the classic, nonlinear, RT bubble-and-spike shape with peak-to-valley amplitude $\eta_{PV} \approx \lambda$. Faint indications of Kelvin–Helmholtz roll-ups are visible at the tip of the spike and along its sides. For the simulations, we use the same mapping scheme in 2D as we did in 1D, only now the Cu–CH_2 interface has a sinusoidal ripple with wavelength $\lambda = 200$ μm and amplitude $\eta_0 = 20$ μm. The run is started at $t = 0$, corresponding to when the drive lasers turn on. By 10 ns, a strong (~15-Mbar) shock has passed through the interface, and the ripple in the Cu has inverted phase due to the Richtmyer–Meshkov instability.[31] By 30 ns, the perturbation has grown with the opposite phase to an overall peak-to-valley amplitude of $\eta_{PV} \approx 180\ \mu m \approx \lambda$, as shown in Figures 4(b) and 4(c). The shape of the perturbation has changed from sinusoidal to bubble-and-spike, indicating that the interface has evolved well into the nonlinear regime. Thus, by 30 ns, we access roughly the same degree of nonlinearity in the laser experiment as that shown for the SN in Figure 2(d) for the 1% velocity perturbation.

The gross features of the experiment are reproduced by both CALE [Figure 4(b)] and PROMETHEUS

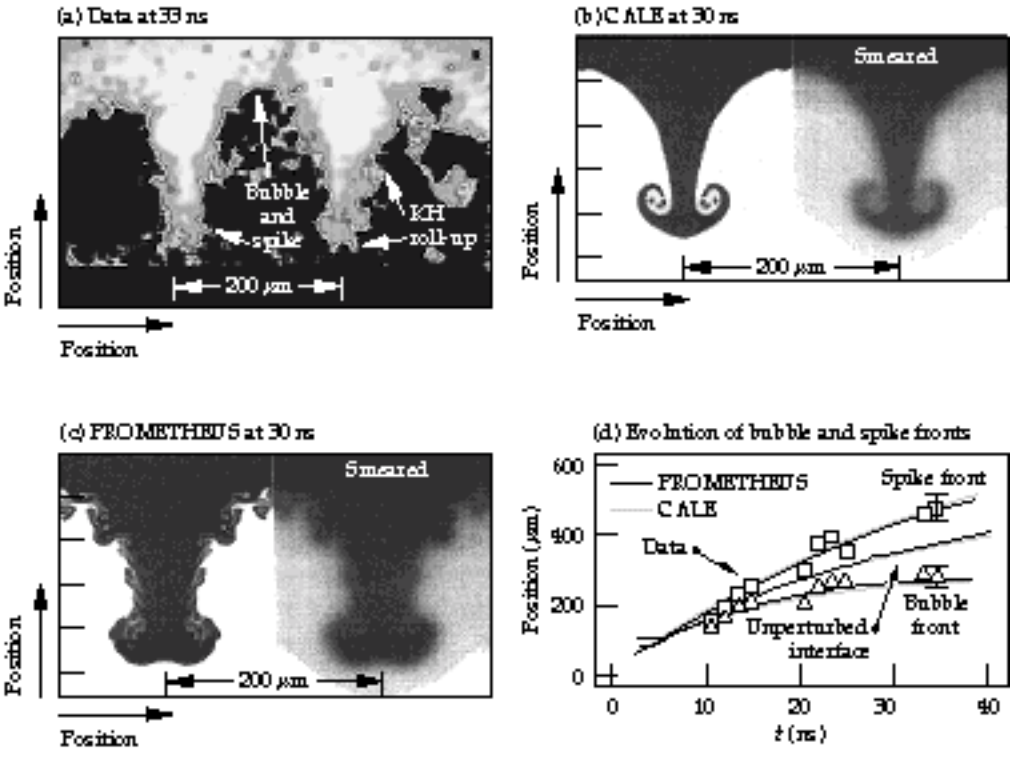

FIGURE 4. Comparison of (a) data at 33 ns with (b) simulations using CALE at 30 ns and (c) PROMETHEUS. The results labeled "smeared" have been convolved with the experimental instrument resolution function. (d) Comparison of the bubble-and-spike front trajectories observed in the data and from the simulations.
(40-00-1296-2756pb01)

[Figure 4(c)] simulations. However, the PROMETHEUS simulation contains more fine structure. When CALE is run in pure Eulerian mode with ideal-gas EOS (not shown), that is, in nearly the same manner as the PROMETHEUS simulation, the two codes give similar results. However, there is still somewhat less fine structure in the CALE result due to interface tracking. Figure 4(d) shows the evolution of the bubble-and-spike fronts, compared with the predictions from both codes. The locations of the 2-D bubble front and spike front are reproduced very well by both hydrodynamics codes. In the frame of reference of an unperturbed interface, both the spike and bubble converge to nearly the same constant terminal velocities, $v_b \approx v_s \approx 3.5$–$4.0$ μm/ns. We compare this with the theoretical asymptotic velocities for the RT instability predicted by Hecht and Alon,[29] namely, $v_{b,s} = [(1/6\pi)2A/(1 \pm A)g\lambda]^{1/2}$, where the + and – in the denominator refer to bubble and spike, respectively. For our conditions of $g \approx 0.35$ μm/ns^2, $A \approx 0.64$, and $\lambda = 200$ μm, the predicted velocities are $v_b = 1.7$ μm/ns and $v_s = 3.6$ μm/ns. Our spike velocities agree with the Hecht–Alon semi-infinite fluid theory, but our bubble velocities are considerably higher. This most likely is due to the finite thickness of the Cu layer. The Cu spike falls into an essentially infinite reservoir of CH_2 plasma, whereas the bubble of CH_2 rises into a thin layer of Cu (thickness ≈ 60 μm $<< \lambda = 200\mu$m), the result of which would be higher bubble velocities.

The study of hydrodynamic instabilities in Type II SNs has broader significance than simply checking a detail in a hydrodynamics calculation. Type II SNs are used in the Expanding Photosphere Method (EPM) for determining the Hubble constant (H_0).[32] This method holds great promise because SNs are bright, allowing a single method to be used to determine distances from tens of kpc to hundreds of Mpc. The basic premise of the EPM is that the light curve—that is, the total emitted flux as a function of time—of a Type II SN can be calculated absolutely, albeit in 1D. By comparing observed brightness of the SN with calculated brightness, one can infer the distance. Applying the EPM to several different SNs at varying distances (D), together with red-shift measurements of the recession velocity (v_{rec}) allows a plot of v_{rec} versus D to be constructed, whose slope is the Hubble constant, H_0. Note, however, that any RT-induced mixing of the radioactive ^{56}Ni and ^{56}Co core outward into the envelope serves as a heat source, potentially altering the light curve.[18] Furthermore, any coupling between the mixing front at the He–H interface and the photosphere could cause the photosphere to become crenulated. The initial blast wave itself may, in fact, have a distorted shape due to Vishniac instabilities,[33] thereby distorting the photosphere from the very beginning. A crenulated photosphere could have a significantly larger surface area than predictions from a 1-D spherical calculation. Furthermore, for a dominant mode $l \geq 20$, as suggested in Figures 1(a) and 2(e), the surface area would look statistically similar regardless of the angle from which the SN were viewed. In other words, *all* Type II SNs with crenulated photospheres would be brighter than assumed based on 1-D spherical calculations. Consider the implications. For a given recession velocity, if SNs were brighter than assumed, they would be further away. This effect decreases the slope of the v_{rec} versus D plot, reducing H_0. Because the age of the universe varies inversely as the Hubble constant ($\tau_{Univ} \sim 1/H_0$), the result of crenulated photospheres due to hydrodynamic instabilities would be an older universe. Experimentally testing any piece of the puzzle, in this case modeling of the SN hydrodynamic instabilities, is indeed a worthwhile pursuit.

Supernova Remnant Formation

SN remnant formation is one of the classic problems of astrophysics, leading to such spectacular objects in the sky as the Crab nebula. With SN1987A, we have the first opportunity to watch the time-dependent dynamics of the early stages of such evolution [see Figure 1(b)].

Figure 5(a) is a schematic of the remnant formation process (taken from Ref. 12). High-velocity SN ejecta sweep up the surrounding ambient plasma, which is left over from the stellar wind of the SN progenitor. At the contact discontinuity (the place where the two plasmas meet), shocks are launched forward into the ambient plasma ("forward shock") and backward into the SN ejecta ("reverse shock"), as illustrated with the 1-D density profile shown in Figure 5(b) (from Ref. 12). When radiation transport and radiative cooling are included in the plasma hydrodynamics, a much higher density is formed in the compressed SN ejecta. The radiation carries heat away, lowering the temperature and pressure, thus making the shocked SN ejecta more compressible. This steepens the density gradient at the contact discontinuity [compare the dashed and solid curves in Figure5(b)]. At the contact discontinuity, pressure and density gradients cross, $P \cdot \rho < 0$, with the lower-density shocked ambient plasma at higher pressure and decelerating the higher-density shocked SN ejecta plasma. Such a situation is hydrodynamically unstable due to the RT instability. This is illustrated in Figure 5(c) (from Ref. 12), which shows strong RT growth at the contact discontinuity. The simulations assumed a $\rho \propto r^{-n}$ ejecta density profile ($n = 6$, 12, 20) flowing into a uniform ambient plasma. Note that qualitatively different mixing evolves, depending on the density profile of the ejecta. The details of what to expect when SN ejecta impact the ring nebula depend on the structure of both the ring and the projectile assembly. Figure 5(d) shows the

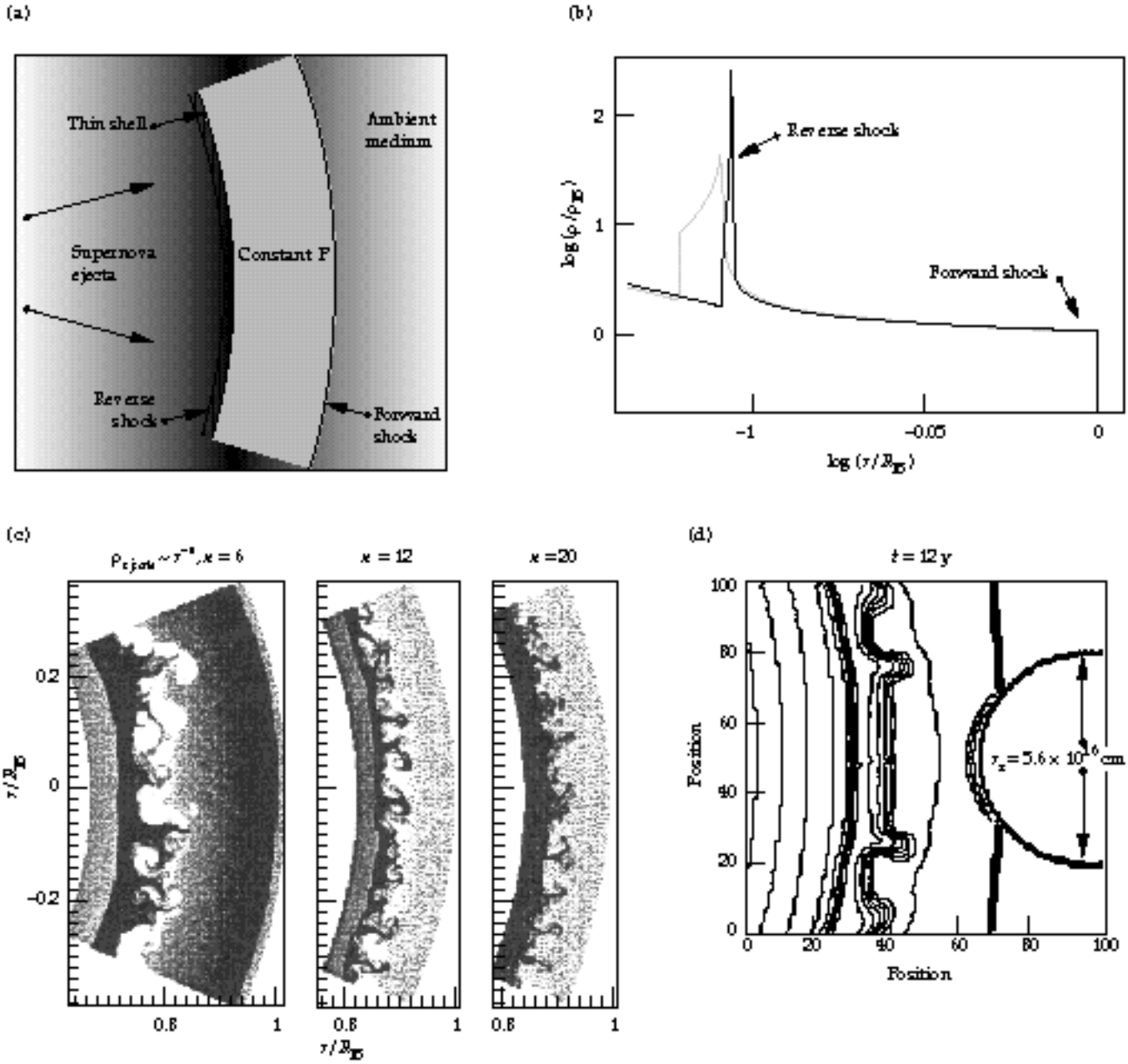

FIGURE 5. (a) Schematic showing the dynamics of SN remnant formation (reproduced from Ref. 12). (b) Structure of a generic SN–stellar-wind interaction (reproduced from Ref. 12). The gray curve shows the structure for small radiative power loss. With larger radiative losses, the stagnated ejecta should collapse to higher density, as the solid curve illustrates. (c) 2-D simulations (from Ref. 12) showing the effect of the ejecta density profile, $\rho_{ejecta} \quad r^{-n}$, on ensuing RT growth at the contact discontinuity. The axes are radius (r) normalized to the position of the forward shock (R_{FS}). (d) 2-D simulation result showing RT instability growth at the contact discontinuity and the imminent collision with the ring (reproduced from Ref. 11). (40-00-1296-2757pb01)

results of a 2-D simulation from a different model (from Ref. 11). Clearly, what transpires depends on whether the contact discontinuity looks like Figure 5(a), 5(c), 5(d), or something completely different. It would be highly beneficial to be able to test these models experimentally prior to the awaited collision.

Hence, our second experiment is focused on testing our understanding of the colliding plasma dynamics in a situation qualitatively similar to that of the ejecta of SN1987A. Our goal is to develop the experiment and model it with the astrophysics codes used to make predictions such as those shown in Figures 1(c), 1(d), 5(c), and 5(d). This work should improve our ability to quantitatively interpret the results of the upcoming pyrotechnics predicted for shortly after the year 2000.

Supernova Remnant Experiment

Our initial approach to experimentally simulate the ejecta–wind interaction hydrodynamics[34] is shown in Figure6(a). We use about 20 kJ of laser energy at a laser wavelength of 0.35 μm, in a 1-ns pulse, to heat a 3-mm-long by 1.6-mm-diam cylindrical Au cavity (a hohlraum) to a temperature of about 220 eV. The x-ray flux ablates a CH plug, doped with Br to reduce the transmission of higher-energy x rays, which is mounted in a 700-μm-diam hole in the hohlraum. The ablation drives a very strong (~50-Mbar) shock through the CH(Br), ejecting plasma at about 30 eV from the rear of the plug. This plasma (the ejecta) expands and cools. The leading edge of the expansion is a high-Mach-number plasma flow (about Mach 10), although it is at well below solid density. The ejecta impact a 700-μm-diam cylinder of aerogel foam located 150 μm away and having a density of 40 mg/cm^3. In response, the flowing ejecta stagnate, and a shock is driven into the foam, as well as back into the ejecta.

We diagnose these experiments by x-ray backlighting at 4.3 keV (Sc He_α) to obtain radiographs of the shocked matter. Figure 6(a) is a 1-D, streaked radiographic image of the target. We show profiles of –ln(exposure) density from the data in Figure 6(c) and from a LASNEX[35] simulation in Figure 6(d), both at t = 6 ns. In both the data and simulation, we observe a clear forward shock in the foam, a reverse shock in the ejecta, and a contact discontinuity in between. From the simulations, the shock breaks out of the CH(Br) at about 2 ns, at which time the back edge of

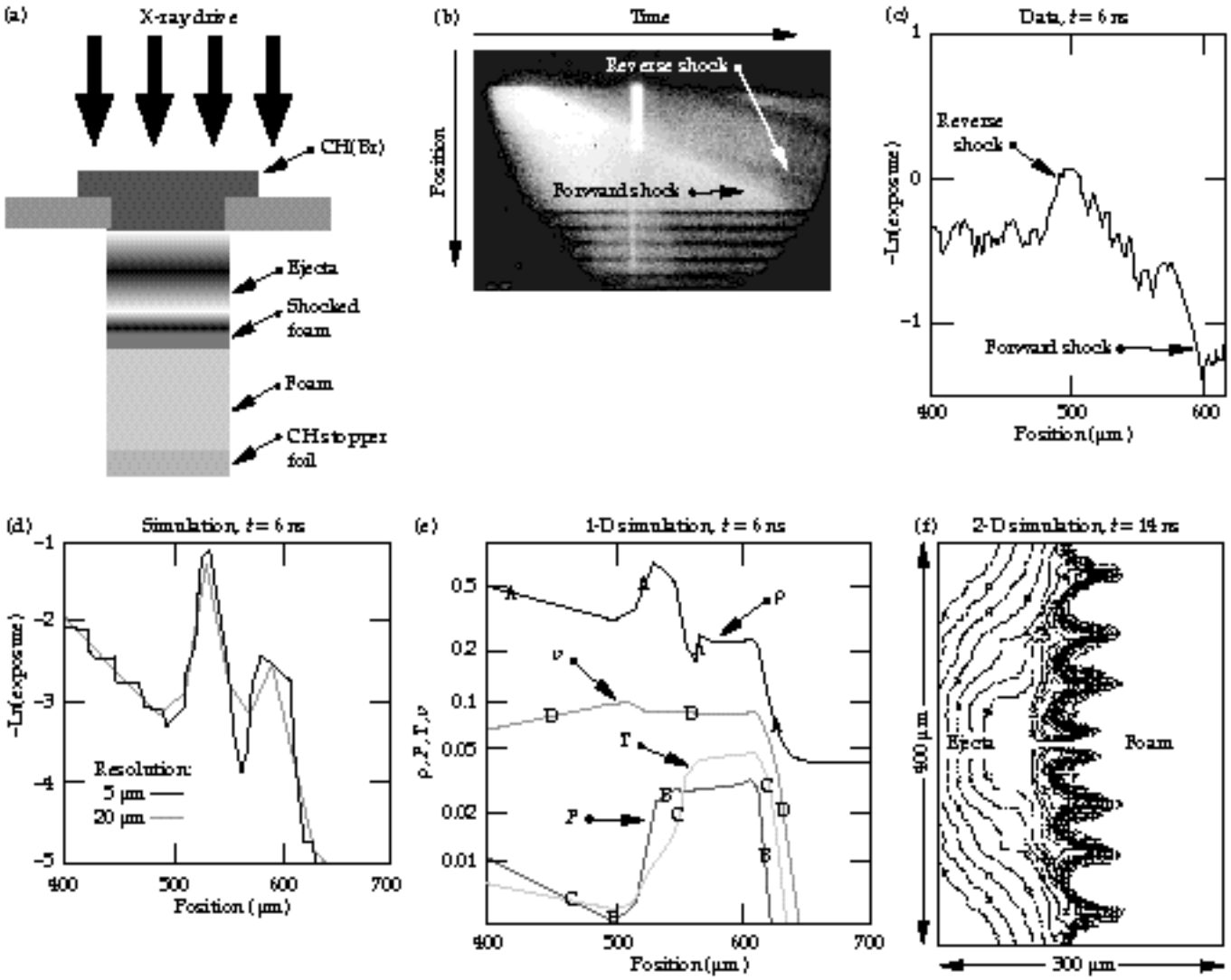

FIGURE 6. (a) Schematic of the laser experiment. (b) Raw streaked image from the experiment. (c) A lineout at 6 ns from the data shown in (b). (d) Same as (c) except based on a 2-D simulation using LASNEX. The solid and gray lines represent different levels of resolution (5 versus 20μm). (e) Profiles from the simulation at 6 ns showing density (g/cm^3), pressure (Mbar), temperature (keV), and velocity (×10^8 cm/s). (f) Isodensity contours at 14 ns from a 2-D LASNEX simulation, showing perturbation growth due to RT instabilities at the contact discontinuity. Ejecta flow into the foam from left to right. (40-00-1296-2758pb01)

the CH(Br) is at a density of about 2 g/cm^3 (compression of ~2), pressure of 45 Mbar, and temperature of 30 eV. The foam is impacted by the ejecta about 1 ns later, suggesting that the high-velocity tail of the ejecta is moving at ~150 μm/ns = 150 km/s. Figure 6(e) shows the density, pressure, temperature, and velocity of the ejecta–foam assembly from the LASNEXsimulation at 6 ns, that is, about 3 ns after the ejecta first start sweeping up the foam. The contact discontinuity is located at a position of about 560 μm in both the data and the simulation, and the peak densities from the simulation on either side of the contact discontinuity in the ejecta (foam) are 0.65 g/cm^3 (0.25 g/cm^3). The pressure is continuous across the contact discontinuity, at a peak value of 0.035 Mbar, the peak temperature is about 50 eV, and the velocity of the projectile assembly is about 1×10^7 cm/s. Both here and in SN1987A, the forward shock driven by the ejecta is a strong shock; that is, the shocked matter is maximally compressed [by a factor of $(\gamma + 1) / (\gamma - 1)$ for a γ-law gas].

The region near the contact surface at the front of the ejecta is RT unstable, as illustrated in Figure 5(c) for SN1987A, and in Figure 6(f) for the laser experiment. In the latter, a seed perturbation of wavelength $\lambda = 50$ μm and initial amplitude $\eta_0 = 1$ μm was imposed on the surface of the foam. By 14 ns, strong RT growth of the perturbation well into the nonlinear regime is visible, due to the $P \cdot \rho < 0$ configuration at the contact discontinuity. The growth bears some semblance to the RT growth shown in Figures 5(c) and 5(d) for the SN ejecta. We intend to apply this experiment to test theories and models being used to predict the behavior of SN1987A well in advance of the upcoming impact of SN ejecta with the ring nebula. Our efforts should facilitate the interpretation of data expected to emerge from the impact.

Conclusions and Future Outlook

We are developing experiments to investigate (1) hydrodynamic instabilities relevant to core-collapse SNs at intermediate times (10^3–10^4 s), and (2) plasma-flow dynamics relevant to the SN ejecta–ambient plasma interactions during the initial stages of remnant formation. Initial results from both experiments look promising. Expanding the first experiment to 3D is the most critical next step to take because RT growth in a supernova is clearly 3D, and growth in 3D is expected to be larger than in 2D.[36] Extending the second experiment into the radiative regime is equally critical because the remnant formation hydrodynamics relevant to SN1987A is clearly radiative.

Beginning such astrophysics experiments now on the Nova laser and other lasers worldwide[33,37,38] is important. With the construction in the U.S. of the ~2-MJ National Ignition Facility laser,[39] and the similar Laser MegaJoule laser[40] planned to be built in France, it is crucial that we acquire experience now with developing laser–plasma astrophysics experiments. Such groundwork will better allow us to plan discriminating astrophysics experiments for the "superlasers" scheduled for completion around the year 2002. This date is just about the time that SN1987A ejecta are predicted to impact the surrounding nebular ring. Dedication ceremonies for the two superlasers may be consummated with a fitting celestial *son et lumière*.

Acknowledgments

Many people have been instrumental in helping this new initiative to get off the drawing boards. We would like to thank E. M. Campbell, J. D. Kilkenny, B. A. Hammel, R. Freeman, D. Dearborn, S. Woosley, T. Weaver, P. Pinto, R. Tipton, J. Colvin, and J. T. Larsen for their assistance along the way. We also thank R. Chevalier for permission to reproduce illustrations from his published work

Notes and References

1. W. D. Arnett, J. N. Bahcall, R. P. Kirshner, and S. E. Woosley, *Ann. Rev. Astron. Astrophys.* **27**, 629 (1989); W. Hillebrandt and P. Höflich, *Rep. Prog. Phys.* **52**, 1421 (1989).
2. E. Müller, B. Fryxell, and D. Arnett, *Astron. Astrophys.* **251**, 505 (1991).
3. B. Fryxell, W. Müller, and D. Arnett, *Astrophys. J.* **367**, 619 (1991).
4. I. Hachisu et al., *Astrophys. J.* **368**, L27 (1991).
5. A. Burrows and B. A. Fryxell, *Astrophys. J.* **418**, L33 (1993).
6. M. Herant and S. E. Woosley, *Astrophys. J.* **425**, 814 (1994).
7. M. Herant, W. Benz, and S. Colgate, *Astrophys. J.* **387**, 294 (1992); *Astrophys. J.* **435**, 339 (1994).
8. H. Bethe, *Rev. Mod. Phys.* **62**, 801 (1990); *Astrophys. J.* **412**, 192 (1993).
9. A. P. S. Crotts et al., *Astrophys. J.* **347**, L61 (1989); E. J. Wampler et al., *Astrophys. J.* **362**, L13 (1990); L. Wang and E. J. Wampler, *Astron. Astrophys.* **262**, L9 (1992); P. Jacobsen et al, *Astrophys. J.* **369**, 63 (1991); and on the internet at web site <http://www.stsci.edu/pubinfo/jpeg/SN1987A_Rings.jpg>.
10. R. McCray, *Ann. Rev. Astron. Astrophys.* **31**, 175 (1993).
11. R. McCray and D. N. C. Lin, *Nature* **369**, 378 (1994); D. Luo and R. McCray, *Astrophys. J.* **379**, 659 (1991); *Astrophys. J.* **430**, 264 (1994).
12. R. A. Chevalier, J. M. Blondin, and R. T. Emmering, *Astrophys. J.* **392**, 118 (1992); R. A. Chevalier and J. M. Blondin, *Astrophys. J.* **444**, 312 (1995).
13. J. M. Blondin and P. Lundqvist, *Astrophys. J.* **405**, 337 (1993).
14. C. L. Martin and D. Arnett, *Astrophys. J.* **447**, 378 (1995).
15. T. Suzuki, T. Shigeyama, and K. Nomoto, *Astron. Astrophys.* **274**, 883 (1993).
16. K. J. Borkowski, J. M. Blondin, and R. McCray, *Astrophys. J.* (in press).
17. J. D. Kilkenny, *Rev. Sci. Instrum.* **63**, 4688 (1992); E. M. Campbell, *Laser Part. Beams* **9**, 209 (1991).
18. T. Shigeyama and K. Nomoto, *Astrophys. J.* **360**, 242 (1990).
19. R. W. Hanuschik and J. Dachs, *Astron. Astrophys.* **192**, L29 (1987); V. M. Blanco et al., *Astrophys. J.* **320**, 589 (1987).
20. F. Witteborn et al., *Astrophys. J.* **338**, L9 (1989); J. Tueller et al., *Astrophys. J.* **351**, L41 (1990); R. McCray, *Ann. Rev. A. Ap.* **31**, 175 (1993).

21. D. Arnett, *Supernovae and Nucleosynthesis* (Princeton Univ. Press, Princeton, NJ, 1996).
22. B. A. Fryxell, E. Müller, and W. D. Arnett, Max Planck Institut für Astrophysik Report 449 (1989).
23. Lord Rayleigh, *Scientific Papers II* (200, Cambridge, England, 1900); Sir Geoffrey Taylor, *Proc. R. Soc. London* **A201**, 192 (1950).
24. B. A. Remington et al., *Phys. Plasmas* **2**, 241 (1995).
25. J. Kane et al., submitted to *Astrophys. J. Lett.* (November 1996).
26. S. G. Glendinning et al., in proceedings of the *Workshop on Laboratory Astrophysics Experiments with Large Lasers*, Eds., B. A. Remington and W. H. Goldstein (February 26–27, 1996), LLNL Rept. No. CONF-960297, p. 18.
27. J. T. Larsen and S. M. Lane, *J. Quant. Spect. Rad. Trans.* **51**, 179 (1994).
28. R. Tipton (author of CALE), private communication (1996).
29. J. Hecht et al., *Phys. Fluids* **6**, 4019 (1994); U. Alon et al., *Phys. Rev. Lett.* **74**, 534 (1995).
30. E. M. Campbell, N. C. Holmes, S. B. Libby, B. A. Remington, and E. Teller, submitted to *Laser Part. Beams* (September 1996); UCRL-JC-124258, Rev. 2 (1996).
31. R. D. Richtmeyer, *Commun. Pure Appl. Math.* **13**, 297(1960); E. E.Meshkov, *Izv. Akad. Nauk SSSR Mekh. Zhidk.Gaza* **4**, 151 (1969) [*Izv. Acad. Sci. USSR Fluid Dynamics* **4**, 101 (1969)].
32. B. P. Schmidt et al.,*Astrophys. J.* **395**, 366 (1992); *Astrophys. J.* **432**, 42 (1994).
33. J. Grun et al., *Phys. Rev. Lett.* **66**, 2738 (1991); G. Schappert et al., in proceedings of the *Workshop on Laboratory Astrophysics Experiments with Large Lasers*, Eds. B. A. Remington and W. H. Goldstein (February 26–27, 1996), LLNL Rept. No. CONF-960297, p. 164.; Ryu and Vishniac, *Astrophys. J.* **313**, 820 (1987); *Astrophys. J.* **368**, 411 (1991); Mac Low and Norman, *Astrophys. J.* **407**, 207 (1993).
34. R. P. Drake et al., in proceedings of the *Workshop on Laboratory Astrophysics Experiments with Large Lasers*, Eds. B. A. Remington and W. H. Goldstein (February 26–27, 1996), LLNL Rept. No. CONF-960297, p. 31.
35. G. B. Zimmerman and W. L. Kruer, *Comments Plasma Phys. Controlled Fusion* **2**, 51 (1975).
36. M. M. Marinak et al., *Phys. Rev. Lett.* **75**, 3677 (1995); G. Tryggvason and S. O. Unverdi, *Phys. Fluids A* **2**, 656 (1990); J. P. Dahlburg et al., *Phys. Fluids B* **5**, 571 (1993); J. Hecht et al., *Laser Part. Beams* **13**, 423 (1995).
37. B. H. Ripin et al., *Laser Part. Beams* **8**, 183 (1990).
38. Y. P. Zakharov et al., in *Plasma Astrophysics* (ESA, 1986), Vol. SP-251, p. 37.
39. J. A. Paisner, E. M. Campbell, and W. J. Hogan, *Fusion Technology* **26**, 755 (1994).
40. CHOCS No. 13, Avril 1995, *Revue Scientifique et Technique de la Direction des Applications Militaires*, CEA; M. Andre, "Conceptual Design of the French LMJ Laser," *First Annual International Conference on Solid State Lasers for Application to ICF*, Monterey, CA, May 31–June 1 (1995), SPIE proceedings.